BIOCHEMISTRY
including biophysical chemistry & molecular biology

Article

pubs.acs.org/biochemistry

Molecular Dynamics Simulation of the Unfolding of Individual Bacteriorhodopsin Helices in Sodium Dodecyl Sulfate Micelles

Venkatramanan Krishnamani and Janos K. Lanyi*

Department of Physiology and Biophysics, University of California, Irvine, California 92697, United States

ABSTRACT: We report molecular dynamics simulations of the trends in the changes in secondary structure of the seven individual helices of bacteriorhodopsin when inserted into sodium dodecyl sulfate (SDS) micelles, and their dependence on the amino acid sequence. The results indicate that the partitioning of the helices in the micelles and their stability are dependent on the hydrophobicity of the transmembrane segments. Helices A, B, and E are stable and retain their initial secondary structure throughout the 100 ns simulation time. In contrast, helices C, D, F, and G show structural perturbations within the first 10 ns. The instabilities are localized near charged residues within the transmembrane segments. The overall structural instability of the helix is correlated with its partitioning to the surface of the micelle and its interaction with polar groups there. The in silico experiments were performed to complement the in vitro experiments that examined the partial denaturation of bacteriorhodopsin in SDS described in the preceding article (DOI 10.1021/bi201769z). The simulations are consistent with the trends revealed by the experimental results but strongly underestimate the extent of helix to extended coil transformation. The reason may be either that the sampling time was not sufficiently long or, more interestingly, that interhelix residue interactions play a role in the unfolding of the helices.

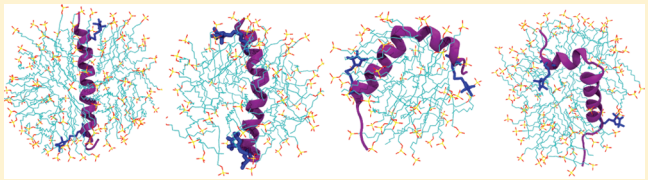

Bacteriorhodopsin (BR) is an integral membrane protein in the cytoplasmic membrane of *Halobacterium salinarum*. The structure of bacteriorhodopsin has been determined to 1.55 Å resolution and reveals a trimer with each monomer consisting of a heptahelical transmembrane bundle and a retinal chromophore in the protein interior attached via a protonated Schiff base to the side chain of Lys-216.[1] A well-described reversible in vitro unfolding−refolding procedure for BR had prompted numerous studies of its refolding.[2−12] The starting equilibrium state is the denatured ensemble of BR in sodium dodecyl sulfate (SDS) micelles along with native lipids from the disrupted bilayer. According to CD spectra in the UV region, this equilibrium state retains ∼50% of the original helical content.[13] This observation poses the question of which of the seven helices or which parts of the helices had become disordered. A better structural description of the SDS-denatured state will facilitate the interpretation and analysis of the in vitro refolding kinetics, which starts from this partially unfolded structure. It will also reveal any variations in the stability of helical segments and/or entire helices and might provide insights into its sequence dependence. An earlier nuclear magnetic resonance (NMR) study of a BR segment that included helices A and B in SDS micelles showed no interproton nuclear Overhauser effect (NOE) between the helices.[14] Because NOE interactions are observed over less than a few angstroms, segments A and B that lie adjacent to one another in the original structure must have become separated in the micelles, while the helical structures were largely conserved. On the other hand, oxidative labeling of methionines has suggested that helices A and D, but not the other five helices, are largely unfolded in SDS micelles.[15]

NMR studies of saposin C had shown that this protein adopts an open conformation with an exposed hydrophobic pocket in SDS micelles.[16] In this system, it was also observed that SDS displaces hydrophobic protein−protein contacts with detergent−protein contacts. Likewise, crystallographic studies of SDS-denatured lysozyme had shown that the detergent molecules intercalate into the hydrophobic core of the protein and "open up" the structure.[17] It seems therefore plausible that SDS inserts between the BR helices and forms stable interactions with hydrophobic residues. If the assumption that there is no protein−protein contact between the TM helices in the micelles is made, the unfolding behaviors of the seven helices may be considered independent of one another. Alternatively, the unfolding behavior of individual helices might be different when they are part of the entire protein.

In this study, each of the transmembrane helices of BR was separately considered for in silico unfolding in SDS micelles. The amino acid sequences of the helices are shown in Figure 1, with positively charged residues colored blue and negatively charged residues red. The goal was to identify the partitioning preference of each TM segment and the specific regions of stability and instability in SDS micelles. This molecular dynamics study was performed to complement and describe the specific events leading to distance distributions of the separation of the ends of each helix in SDS micelles, as determined by DEER spectroscopy (DOI 10.1021/bi201769z).

Received: November 30, 2011
Revised: January 18, 2012
Published: January 23, 2012

ACS Publications © 2012 American Chemical Society

Figure 1. Sequence of residues of each individual helix used in the simulations. Positively charged residues are colored blue and negatively charged residues red. The helices are color-coded to be consistent with the rest of the figures.

MATERIALS AND METHODS

Setup of the Simulation Box, Equilibration, and Simulation of Production. The coordinates of the seven TM helices of BR (A–G) were extracted from the crystal structure (Protein Data Bank entry 1C3W).[1] In some of the simulations, a cysteine-attached MTSL spin-label was introduced into appropriate sites (the ends of the helix) in each TM helical fragment using PyMOL,[18] to comply with the location of the spin-labels in our experimental system (DOI 10.1021/bi201769z). The dihedral angles for each MTSL spin-label with Cys were modeled according to the dihedral angles obtained for its configuration at the minimal potential.[19] The charged residues (Arg, Lys, Glu, Asp, and His) were appropriately protonated or deprotonated for a system at pH 7 based on the pK_a of the side chains in solution, because we expected these groups to experience exposure to water at least part of the time during the conformational fluctuations of the peptides.

Given that all the helices of BR are composed mainly of highly hydrophobic residues, with the exceptions of specific hydrophilic residues essential for its function as a light-driven proton pump,[20−23] the helices are expected to be in an energetically favorable SDS micelle-embedded state. SDS molecules (120) were added to surround the TM segments in a toroidal arrangement, using a custom script. This structure was energy minimized in vacuum using the l-bfgs or conjugate gradient algorithm to remove overlapping and close contacts between the atoms. Then, SPC216[24,25] type water molecules were added to fill the simulation box (Table 1). The SDS concentration in the simulation box is approximately 0.5 M. Sodium and chloride ions were added to the system to create a NaCl concentration of 100 mM. Additional sodium ions were added to neutralize the negative charges on the SDS headgroups in the simulation box. This solvated neutral system was then energy minimized to relax and remove steric conflicts between the atoms, using the l-bfgs algorithm. The dimensions of the equilibrated simulation box and number of atoms in each simulation box are listed in Table 1.

A 5 ns simulation was performed on the resulting system at 300 K with harmonic position restraints (force constant of 1000 kJ mol^{-1} nm^{-2}) on the backbone atoms of the peptide in a *NVT* ensemble to equilibrate SDS and solvent molecules around the peptide. The electrostatic interactions were calculated using the particle mesh Ewald (PME) method,[26,27] with a 0.9 nm cutoff. A cutoff of 1.4 nm was used for Lennard-Jones interactions. During equilibration, the system was weakly coupled to a Berendsen thermostat[28] at 300 K with a coupling time constant (τ_T) of 0.1 ps.

Starting from the equilibrated structure, the production simulations were performed at constant temperature, pressure, and number of particles (*NPT*). There were no constraints applied, and all atoms were freely simulated in the box. The production runs had their temperature coupled separately for protein and SDS and for solvent and ions using an extended ensemble Nose-Hoover scheme[29,30] at 300 K with a τ_T of 0.5 ps. The initial velocities were again generated using a random Maxwell distribution at 300 K. The pressure of the system was isotropically coupled at 1 bar with a compressibility of 4.5 × 10^{-5} bar^{-1} using a Parrinello-Rahman barostat[31] with a τ_p of 5 ps. The LINCS algorithm was used to constrain all the bond lengths during all simulation steps except for energy minimization.[32,33] A 2 fs time step was used during equilibration and production runs.

Table 1. Contents and Dimensions of the Simulation Box[a]

helix	N_{total}	N_{water}	N_{SDS}	N_{NA}	N_{CL}	N_{agg}	box size (nm)
A	39658	12383	120	141	23	109	7.56 × 7.56 × 7.54
B	39627	12375	120	144	23	68	7.56 × 7.56 × 7.53
C	39623	12366	120	149	27	99	7.54 × 7.54 × 7.52
D	39657	12393	120	145	23	52	7.55 × 7.55 × 7.52
E	39677	12370	120	141	23	100	7.55 × 7.55 × 7.52
F	39620	12347	120	141	23	87	7.55 × 7.55 × 7.52
G	39578	12338	120	146	27	87	7.55 × 7.55 × 7.52
D mutant	39607	12374	120	148	27	74	7.55 × 7.55 × 7.52

[a]Abbreviations: N_{total}, total number of atoms; N_{water}, number of water molecules; N_{SDS}, number of SDS molecules; N_{NA}, number of sodium ions; N_{CL}, number of chloride ions; N_{agg}, aggregation number of SDS molecules around the helix at 100 ns; box size, dimensions of the simulation box.

Force Field Parameters and Analysis of Trajectories. GROMACS was used in this molecular dynamics study to perform all simulations. The GROMOS87 united atom force field was the choice in our setup because the GROMOS96 force field parameters generated from the PRODRG server (http://davapc1.bioch.dundee.ac.uk/programs/prodrg/)[34] were not stable in the stability test simulations (data not shown). The GROMOS87 force field (ffgmx force field) was used for the protein with SPC water model.[24,35] The force field parameters in GROMOS87 format for SDS were initially generated using the PRODRG server.[34] Because these parameters were not sufficiently stable in our SDS micelle simulations, we modified our parameters on the basis of the SDS parameters of Sammalkorpi et al.[36] and Schweighofer et al.[37] The GROMOS96 parameters of the MTSL spin-label were

dx.doi.org/10.1021/bi201770y | *Biochemistry* 2012, 51, 1061−1069

kindly provided by H. J. Steinhoff from the University of Groningen (Groningen, The Netherlands). The MTSL parameters in GROMOS96 format were converted to GROMOS87 format for consistency in the force field with parameters for SDS and protein. To convert from GROMOS96 to GROMOS87, the bond stretching constants were modified from a fourth-power potential to a harmonic potential and angle potential values were modified from a cosine-based potential to a harmonic potential as described in sections 4.2.1 and 4.2.5 of the GROMACS 4 user manual.[38]

The trajectory was sampled every 4 ps for 100 ns for all the analyses unless mentioned otherwise. Analysis tools provided with the GROMACS package and custom scripts were used for all the analyses. VMD,[39] PyMol,[18] and a Tachyon ray tracer were used to visualize the simulation and to generate the images. These simulations were conducted on a single Intel Core2 Quad 2.4 GHz processor with four threads or on an AMD Phenom II X4 940 3 GHz processor again running four threads.

RESULTS

The equilibrium SDS aggregation number at 298 K obtained from time-resolved fluorescence quenching measurements of 0.44 M SDS in a solution with an ionic strength of 100 mM is 109.[40] A molecular dynamics study of SDS molecules at a concentration of 700 mM at 323 K provides micelles of 50−70 SDS molecules.[36] The SDS micelle aggregation number observed in our simulation setup had average values between 52 and 109 SDS molecules at 300 K and 500 mM SDS, sampled at 100 ns, after sufficient equilibration of the system (Table 1). The SDS micelle aggregation numbers in these simulations are comparable with those reported when the effect of the hydrophobicity of the inserted protein on the SDS aggregation numbers is taken into account.

We find that the molecular dynamics simulations of the TM domains in SDS micelles show a remarkable correlation of the partitioning of the peptides into the micelles with their amino acid sequences, their hydropathy plots, and the consequent secondary structure changes. The observed changes in these parameters for each of the seven helices are discussed below.

Helix A. The spatial distribution of helix A over the simulation shows a strong preference of the entire structure to remain within the hydrophobic core of the SDS micelles (Figure 2A). Only the N- and C-terminal residues are exposed and interact with water molecules (water not shown for the sake of clarity). An NMR structure for this helix[14] had revealed that it retains all of its native helicity in the SDS micelles, as in our simulations where we observe that helix A is one of the least perturbed in its structural deviation from the native starting structure (Figure 3A). As a simple measure of conformational flexibility of the TM segments in the SDS micelles, root-mean-square fluctuations (rmsf) of α-carbons of each residue were calculated over the simulation time (Figure 4B). The average residue rmsf for helix A over the entire helix is low, 1.4 Å. The hydropathy plot (Figure 4A) of the sequence of helix A generated using MPEx[41] based on the octanol scale (window size 5)[42] revealed that the side chains of helix A are mostly hydrophobic (Figure 1), with charged residues at the helical ends. Polar residues in the central region of the helix seem to have no effect on the rmsf, i.e., the structural stability in the surrounding regions. The hydropathy values around the polar residues are below zero, but the regions remain in the micellar core. The secondary structure of the helices was

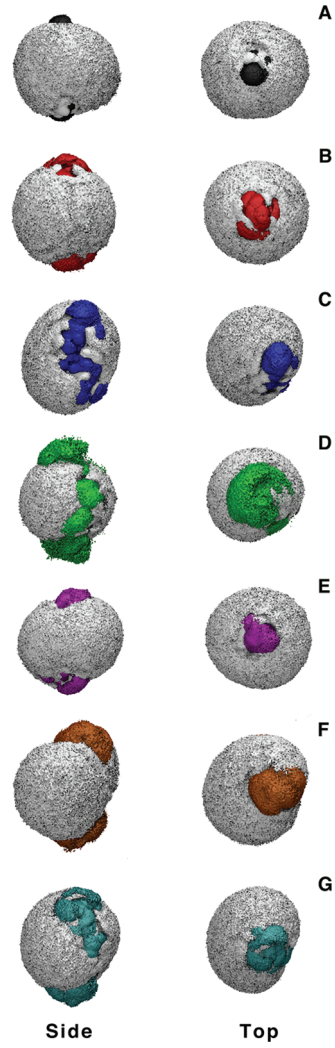

Figure 2. Spatial distribution of SDS molecules (white) and helices (color-coded as in Figure 1), averaged over the entire simulation. The various helices of BR [helix A (black), helix B (red), helix C (blue), helix D (green), helix E (magenta), helix F (orange), and helix G (cyan)] show different partitioning preferences in the SDS micelles. The visible regions of the protein are in contact with water (latter not shown for the sake of clarity).

calculated using the DSSP algorithm developed by Kabsch and Sanders[43] over the entire simulation time. For helix A, it shows (Figure 5A) that all of the initial helical structure is retained, with several short-lived random coil regions induced at the C-terminus during the course of the simulation. This increases the flexibility and the rmsf of α-carbon atoms from the C-terminal region of helix A from ∼0.2 to ∼1 Å for the rest of the helix. The N-terminus retains its secondary structure and remains more or less similar to that of the starting state throughout the simulation.

Helix B. Helix B also remains within the micellar core, as a result of a hydrophobic TM sequence (Figure 2B) and a favorable hydropathy profile (Figure 4A). In the NMR structure, helix B revealed a slight kink at Pro-50 with altered ϕ and ψ angles of Thr-47 and Leu-48,[14] and we observe a similar kink in our simulations (Figures 3B and 4, red curve). Similar to helix A, helix B shows very little backbone fluctuation, with an average peptide rmsf of 1.8 Å. This helix contains three charged residues at the N-terminus. The TM

dx.doi.org/10.1021/bi201770y | Biochemistry 2012, 51, 1061−1069

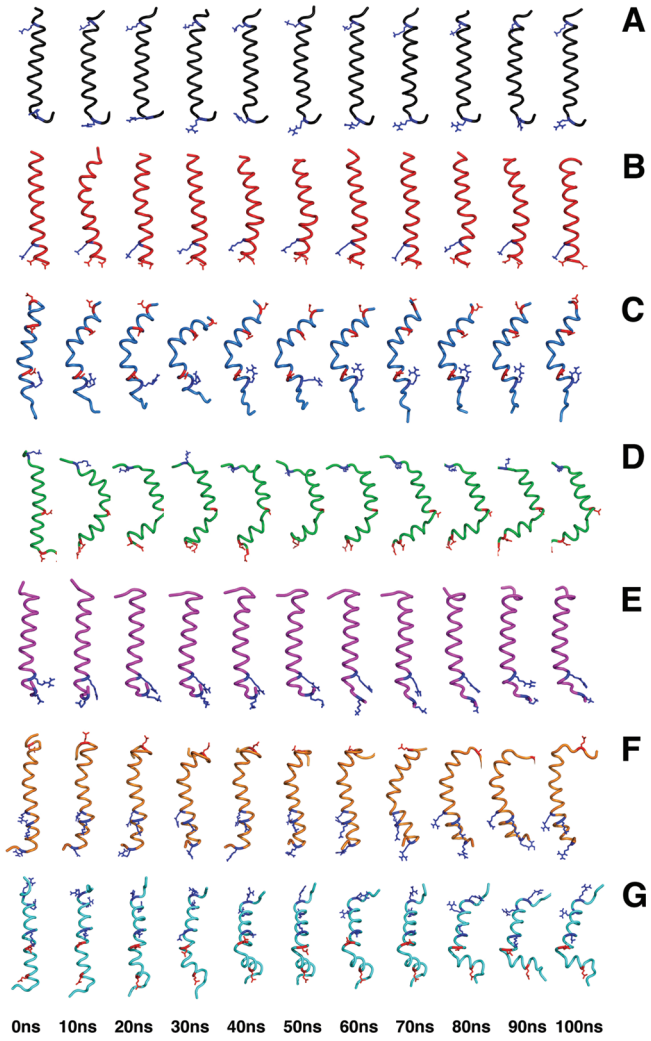

Figure 3. Snapshot of the TM segment in SDS micelles every 10 ns for 100 ns of the simulation time. The protein backbones of helix A (black), helix B (red), helix C (blue), helix D (green), helix E (magenta), helix F (orange), and helix G (cyan) are shown in cartoon representation along with negatively (red) and positively (blue) charged residues shown as sticks.

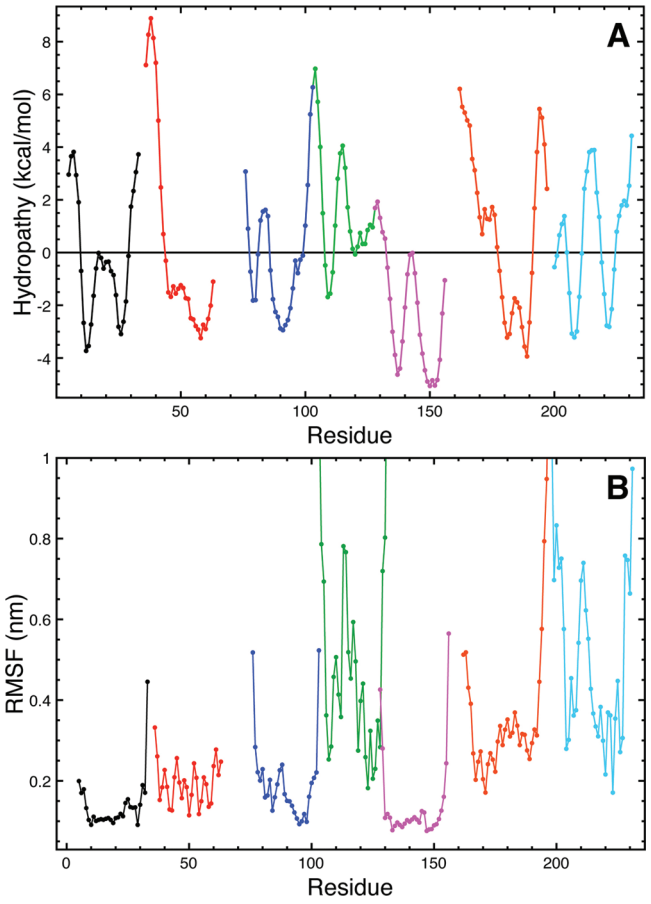

Figure 4. (A) Hydropathy plot of BR using the Whimley and White octanol scale.[42] (B) Root-mean-square fluctuation (rmsf) of each residue of BR averaged over 100 ns with a sampling rate of 4 ps and compared with the starting structure. Helix A (black), helix B (red), and helix E (magenta) show the least fluctuation with rmsf values of <2 Å (the dotted line represents the average rmsf over all residues). Helix C (blue), helix D (green), helix F (orange), and helix G (cyan) have rmsf values of >3.5 Å.

segment is mostly hydrophobic, with no charged residues and two relatively polar Thr residues at positions 46 and 47 (Figure 1). It retains most of its initial helicity, except for a turn/bend formed in the region that immediately precedes Pro-50 at 40 ns (Figure 5B).

Helix C. In contrast to helices A and B, helix C partitions to the SDS micelle−water interface. One side of the helix face exhibits extensive interactions with the SDS sulfate groups and water molecules, and the opposite face interacts with the hydrophobic core of the micelle (Figure 2C). The structural flexibility all along the helix remains comparable with that of helices A and B that remain inside the micellar core. Helix C displays a prominent bend near the central part of its TM segment (Figure 3B). This increased local flexibility (Figure 4B, blue curve) correlates with a positive peak in the hydropathy plot (Figure 4A, blue curve). The positively charged Arg-82 and the anionic Asp-85 are located in the regions of increased flexibility of the peptide backbone. This flexibility culminates in the formation of a loop in the 100 ns time course of the simulation (Figure 5C).

Helix D. Similar to helix C, helix D partitions to the interface of the micelle (Figure 2D). It exhibits a prominent bending around residues Val-112, Gly-113, Ala-114, Asp-115, and Gly-116 (average peptide rmsf of 5.4 Å) (Figure 3D). Helix D contains two Asp residues a Lys near its N-terminal end, a single Lys on the C-terminal end, and a single Asp near the center (Figure 1). The location of the structural perturbation correlates with the positive peak in the hydropathy plot, i.e., mainly with Asp-115 (Figure 4A,B). From Figure 5D, the C-terminus (approximately three to five residues) is unfolded to a random coil state, whereas the N-terminus retains its initial conformation. Asp-115 at the center of the segment interacts with polar molecules, allowing competition between the inter-residue hydrogen bonding network and polar molecules. Conceivably, this is what destabilizes the helical structure into a turn and induces a nearly 90° kink (Figure 3D).

Helix E. The absence of charged residues in the TM segment of helix E (Figure 1) ensures that the segment remains in the micelle core (Figure 2E), with minimal structural perturbation (Figures 3E, 4B, and 5E). The peak in the hydropathy plot due to the presence of Ser-141, Thr-142, and Met-145 does not seem to affect the partitioning or the

dx.doi.org/10.1021/bi201770y | *Biochemistry* 2012, 51, 1061−1069

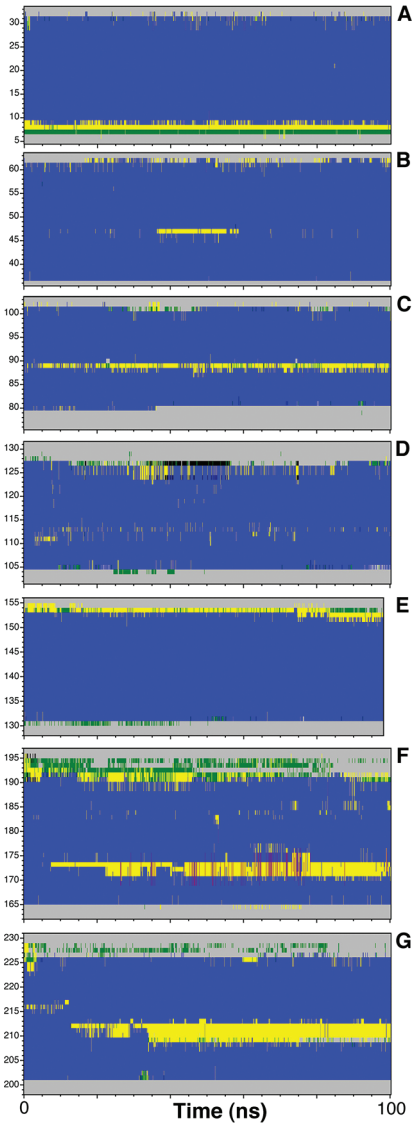

Figure 5. Time course of the secondary structure of each helix in SDS micelles from 0 to 100 ns as calculated from the dssp algorithm.[43] The color codes are as follows: blue for helix, yellow/green for turn/bend, and gray for random coil. The N-terminus is located at the bottom of each graph with the C-terminus at the top.

structural rigidity of the helical segment in the SDS micelle (Figure 4A,B).

Helix F. Helix F partitions more toward the aqueous micelle interface than helices A, B, and E, with considerable interaction of its ends with polar molecules (Figure 3F). The segment contains four charged residues: two Arg's, a Lys, and a Glu. Two of these are within the TM stretch of the helix. The N-terminus of the helix has one positively charged residue and the C-terminus a negatively charged residue. This helix exhibits structural perturbation all along its length (Figure 4B). Figure 5F shows the loss of secondary structure at the Arg and Lys residues near the middle of the TM segment. The C-terminal end unfolds into an apparently completely random coil. In contrast, the N-terminal end retains its secondary structure, which is comparable to that of the initial state. This helix displays the greatest degree of flexibility observed in this study, with an average rmsf of ~5–6 Å for all the residues.

Helix G. Helix G contains five charged residues, one Glu and two Arg's on the ends and one Asp and one Lys at the center of the TM segment (Figure 1). It partitions to the micelle interface, like helices C and D (Figure 2G). Helix G exhibits pronounced bending, similar to that of helices D and C, at Leu-211, Asp-212, Val-213, and Ser-214 (Figure 3G). Consistent with what was observed with other helices, as well, the positive peak in the hydropathy plot correlates with an increased local structural flexibility (Figure 4A,B). The C-terminal and N-terminal ends of this helix unfold and assume a turn/bend structure during the simulation.

Helix D (consequences of the D115L replacement). The results of the simulations of the perturbation of helical structure at charged residues in the TM segments are consistent with the finding that Asp-115 increases the extent of deuterium–hydrogen exchange in helix D.[44] We tested the effect of the loss of a charged residue in the TM region by replacing Asp-115 with Leu.

The modified helix remains in the micellar core (Figure 6A), in contrast to the spatial distribution of wild-type helix D, which

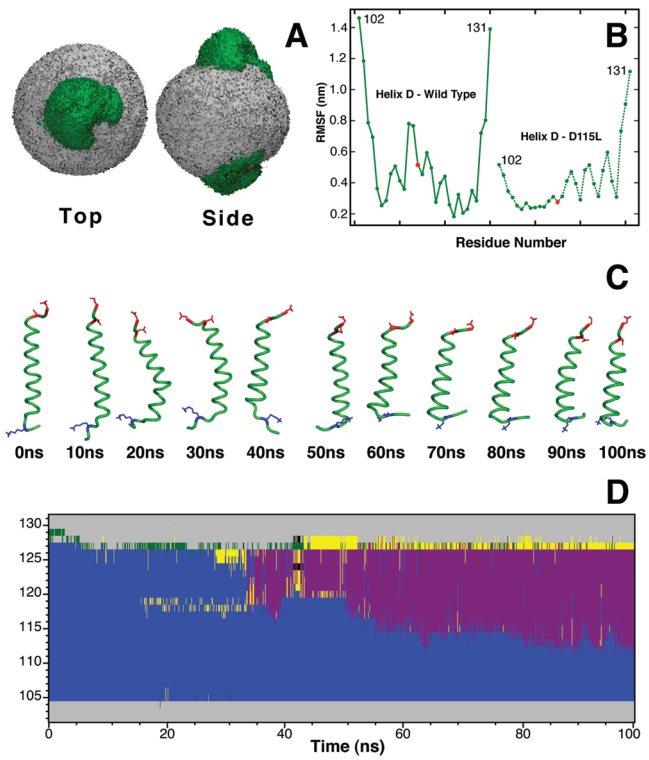

Figure 6. Analysis of the effect of the D115L mutation on helix D. (A) Spatial distribution of SDS micelles and the helix. (B) Comparison of the rmsf's of α-carbons for helix D in D115L and the wild type (position 115 marked in red). (C) Snapshot of the peptide backbone every 10 ns for 100 ns. (D) Time course of secondary structure changes of the peptide.

shows interaction of one side of the helix with water and headgroups of SDS (Figure 2C). The rmsf of the α-carbon exhibits reduced flexibility around residue position 115 when compared to its wild-type counterpart (Figure 6B) and reveals greater structural rigidity and preservation of helical structure (Figure 6C). The C-terminal half of the mutated helix progressively converts from the C-terminus to an unusual five-residue turn helical stretch (Figure 6D, between ~35 and 100 ns).

dx.doi.org/10.1021/bi201770y | *Biochemistry* 2012, 51, 1061–1069

Spin−Spin Distance Distribution. We calculated distributions for the separation between the nitrogen atoms of the nitroxides of pairs of spin-labels at the extremities of each helix, to simulate experimental results from the preceding paper (DOI 10.1021/bi201769z). They are shown in Figure 7 (bold lines). This distribution is compared to the experimentally obtained double electron−electron resonance (DEER) distance distributions for spin-labels on the helices in the denatured state (Figure 7, dashed lines). Unlike the MD simulations that examine single helices in the micelles, the DEER experiments were conducted with the entire protein. The simulated distance distributions (Figure 7, bold lines) partly reproduce the trend in the DEER distance distributions in the denatured state (Figure 7, dashed lines) but miss entirely the spread of the end-to-end distance distribution. In other words, the heterogeneity of structure in the denatured protein in experiments was not observed in the simulations.

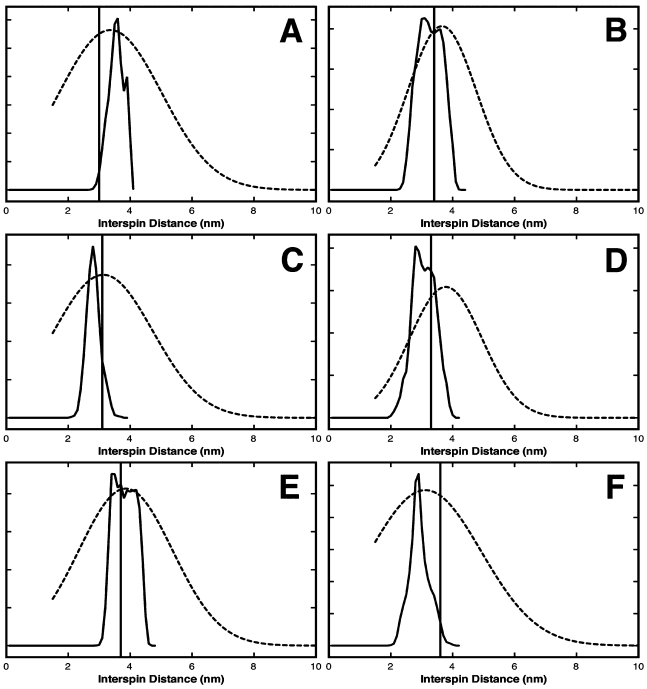

Figure 7. Interspin distance distribution calculated between nitrogens of the two nitroxides in doubly labeled helices from simulations (bold lines) compared with distributions obtained from DEER experiments (dotted lines). The distributions for helix A (A), helix B (B), helix D (C), helix E (D), helix F (E), and helix G (F) are shown. The vertical bold lines indicate the Cβ−Cβ distances of the labeled residue positions in the crystal structure of BR. The spin−spin distance distribution of helix C is not shown here because the corresponding mutant protein could not be expressed in sufficient quantity, and a DEER experimental distance distribution could not be obtained.

DISCUSSION

Helices A, B, and E are fully embedded in the micelle core, interact with the SDS hydrocarbon tails (Figure 2), and retain almost 100% of their initial helicities (Figures 3 and 5) throughout the course of the simulation. This is consistent with the notion that SDS molecules promote and stabilize helices. In contrast, helices C, D, F, and G are found to interact with the polar SDS headgroups and water molecules at the micelle interface (Figure 2). The observation suggests that the partial unfolding of these helices in SDS micelles may be the consequence of how they partition in the micelles.

In helix D of BR, mutating the Asp residue at position 115 to an Ala residue had been found to result in lower levels of deuterium−hydrogen exchange of the peptide in SDS micelles compared to the wild type, but replacing a polar residue, Thr at position 90, with an Ala did not.[44] This observation demonstrated that partitioning of the TM segments in the SDS micelles can be driven by the presence of a single charged residue in the hydrophobic segment; otherwise, polar versus nonpolar differences have a weaker effect. Experimental results with synthetic TM peptides in SDS had indeed suggested interfacial partitioning when a single Asn residue was introduced in the middle of the α-helical segments.[45] An extensive study of designed TM helices in a lipid bilayer also pointed to the transverse orientation of the helices to the membrane normal when hydrophilic or charged residues were introduced into the segments.[46]

In our simulation study, the D115L mutation in helix D presents additional evidence that loss of a charged residue affects the partitioning of the helix in SDS micelles (Figure 6). The observation that the C-terminal half of mutated helix D displays a tendency to form α-helix is more likely the result of the structural preference of the C-terminal sequence when embedded in SDS micelles rather than the effect of the D115L mutation. This tendency was not observed in wild-type helix D possibly because of the partitioning of the helix to the micelle interface and partial unfolding of the helix.

It was previously observed that lowering the pH from 6 to 4, i.e., to below the pK_a of carboxyl side chains, resulted in increase in the α-helix content of BR fragments C−D and F−G.[47] These results strongly suggest that in the micelles the side chains interact with water, and the side chain charges influence the partitioning of the helix in SDS micelles and the secondary structure. Indeed, we observe the destabilized regions of the TM segment in SDS micelles always at the locations of charged amino acids, as in the case of helices C, D, F, and G (Figures 3−5). Comparing the hydropathy plots (Figure 4B) with residue rmsf values (Figure 4A) reveals a striking correlation of increased conformational flexibility of the backbone with the location of charged residues. Consistent with the earlier experimental results,[44] polar but uncharged residues like Thr and Ser do not affect the stability of the backbone. This suggests the possibility that hydropathy plots can be used to predict the partitioning and the possible locations of unfolding of the TM helices (Figures 4A,B).

Comparing the partitioning preference of the helices in SDS micelles and the conformational flexibility in terms of the rmsf of residues (Figures 2 and 4), we find it is evident that TM segments fully embedded in the micelle structure with little or no interaction with sulfate headgroups of SDS and/or water molecules adopt a more stable conformation than segments that significantly interact with these polar molecules. This observation supports the notion that SDS micelles have a stabilizing effect on helical peptides[48−51] and can be rationalized in terms of a combination of hydrophobic and electrostatic interactions. To become isolated from the aqueous environment, the hydrophobic side chains interact with the lipid tails of the SDS micelles, leading to the formation of a stable helix in that region. The presence of a charged residue, in contrast, places the helix at the interface to hydrate the charge (Figure 5). The result is destabilization of the helices, and above average rmsf values within the helix were observed in

helices D, F, and G. The sharp unfolding of the locality of charged residues seen in helices D and G is not observed in helix F, however. Instead, the entire backbone of helix F appears to have become flexible.

Helices F and G are observed to be the most unstable of the seven helices in SDS. The instability of the two C-terminal helices was observed by Luneberg et al.,[47] the least helical content being that of the F−G interhelix hairpin in SDS micelles among the rest of the helices estimated by CD spectroscopy. The results of this study illustrate that the presence of charged residues in the hydrophobic TM segment of the helices (F and G) drives the helix partitioning preference to the micelle interface, and the interactions of the residues with polar molecules destabilize the helix at the location of the charge.

Spin-labels have considerable internal conformational flexibility because of the rotations of the bonds tethering the nitroxide to the backbone of the protein. The various rotamers of the spin-label contribute to the width of the distance distribution observed in the simulation (Figure 7). The width of the distribution is expected to vary between samples according to the restrictions imposed on the internal bond rotations of the spin-label by steric conflicts. A shift of the mean interspin distance in the SDS micelles to higher values compared to the native distance in the crystal structure suggests an extended coil caused by partial unfolding of the helix between the two spin-labels attached to the ends of the segments. Conversely, a shift of the mean distance to lower values suggests a kink or bend in the helix segment because of increased flexibility that would be the result of local unfolding.

The kinks observed in helices B, C, and F in SDS micelles are in the region of the proline residues. It was Son et al. who had previously observed, in a simulation study of BR helices embedded in a continuum bilayer potential, that the relative thickness of the bilayer with respect to the helix length influenced the degree of kinks in the helices.[52] Because SDS micelles exhibit a more fluid and flexible hydrophobic core than bilayers, we would expect the location and arrangement of the kinks in helices B, C, and F to be heterogeneous. They should be influenced by a combination of interlinked factors, such as SDS micelle aggregation number, partitioning of the helix to the micellar interface, charged residue-influenced unraveling of the helical regions, and the proline residue-induced breaks in the helical structure.[53]

The distance distribution of interspin distances obtained from simulations does not exactly reproduce the end-to-end helix distance distributions obtained from DEER experiments (DOI 10.1021/bi201769z). As shown in Figure 7, in the case of helices A, D, F, and G, the simulation reveals a trend in the direction of collapse or extension of the majority population of helices in the SDS micelle obtained from experiments, but for helices B and E, the simulation produces less collapse than what was found experimentally (the DEER experiments did not include helix C). A possible reason for the incomplete reproduction of the experiments might be that the 100 ns time scale of the simulations is not sufficient for sampling all the conformations of the unfolded equilibrium ensemble in SDS micelles. Additionally, the heterogeneity of the structural states (broad distance distribution) observed in the distance distributions from the DEER experiments is not evident in the simulations. This might be a consequence of side chain interactions that occur between the helices in the DEER experiments with the complete protein but not in the simulations of the single helices. There is reason to entertain such a possibility. While the persistence of helices B and E and the unfolding of helix D in SDS, as individual helices, are in accord with the conclusions about these segments reached from oxidative labeling of methionines in the whole protein,[15] and in the case of helix B also from NMR,[14] the results for other helices are in disagreement. Importantly, NMR indicates no unfolding for helix A in SDS when in the A−B segment with the rest of the protein absent. The two experimental results, and the MD simulation, for helix A at least, could be reconciled if this helix unfolded only in the whole protein. This would imply that in SDS micelles interhelix side chain interactions can stabilize unfolded structures.

AUTHOR INFORMATION

Corresponding Author

*E-mail: jklanyi@uci.edu. Phone: (949) 824-7150.

Funding

This study was supported by grants to J.K.L. from the National Institutes of Health (5R37GM029498) and the U.S. Department of Energy (DEFG03-86ER13525).

Notes

The authors declare no competing financial interest.

ACKNOWLEDGMENTS

We thank Dr. Alfredo Freites for his valuable discussions.

ABBREVIATIONS

BR, bacteriorhodopsin; SDS, sodium dodecyl sulfate; TM, transmembrane; DEER, double electron−electron resonance; MD, molecular dynamics; MTSL, (1-oxyl-2,2,5,5-tetramethyl-pyrolinyl-3-methyl)methanethiosulfonate; rmsf, root-mean-square fluctuation.

REFERENCES

(1) Luecke, H., Schobert, B., Richter, H. T., Cartailler, J. P., and Lanyi, J. K. (1999) Structure of bacteriorhodopsin at 1.55 Å resolution. *J. Mol. Biol. 291*, 899−911.

(2) Booth, P. J., Flitsch, S. L., Stern, L. J., Greenhalgh, D. A., Kim, P. S., and Khorana, H. G. (1995) Intermediates in the folding of the membrane protein bacteriorhodopsin. *Nat. Struct. Biol. 2*, 139−143.

(3) Booth, P. J., Farooq, A., and Flitsch, S. L. (1996) Retinal binding during folding and assembly of the membrane protein bacteriorhodopsin. *Biochemistry 35*, 5902−5909.

(4) Sugiyama, Y., and Mukohata, Y. (1996) Dual roles of DMPC and CHAPS in the refolding of bacterial opsins in vitro. *J. Biochem. 119*, 1143−1149.

(5) Booth, P. J., Riley, M. L., Flitsch, S. L., Templer, R. H., Farooq, A., Curran, A. R., Chadborn, N., and Wright, P. (1997) Evidence that bilayer bending rigidity affects membrane protein folding. *Biochemistry 36*, 197−203.

(6) Booth, P. J. (1997) Folding α-helical membrane proteins: Kinetic studies on bacteriorhodopsin. *Folding Des. 2*, R85−R92.

(7) Riley, M. L., Wallace, B. A., Flitsch, S. L., and Booth, P. J. (1997) Slow α helix formation during folding of a membrane protein. *Biochemistry 36*, 192−196.

(8) Curran, A. R., Templer, R. H., and Booth, P. J. (1999) Modulation of folding and assembly of the membrane protein bacteriorhodopsin by intermolecular forces within the lipid bilayer. *Biochemistry 38*, 9328−9336.

(9) Lu, H., and Booth, P. J. (2000) The final stages of folding of the membrane protein bacteriorhodopsin occur by kinetically indistinguishable parallel folding paths that are mediated by pH. *J. Mol. Biol. 299*, 233−243.

(10) Allen, S. J., Kim, J. M., Khorana, H. G., Lu, H., and Booth, P. J. (2001) Structure and function in bacteriorhodopsin: The effect of the interhelical loops on the protein folding kinetics. *J. Mol. Biol. 308*, 423−435.
(11) Compton, E. L., Farmer, N. A., Lorch, M., Mason, J. M., Moreton, K. M., and Booth, P. J. (2006) Kinetics of an individual transmembrane helix during bacteriorhodopsin folding. *J. Mol. Biol. 357*, 325−338.
(12) Lu, H., Marti, T., and Booth, P. J. (2001) Proline residues in transmembrane α helices affect the folding of bacteriorhodopsin. *J. Mol. Biol. 308*, 437−446.
(13) Huang, K. S., Bayley, H., Liao, M. J., London, E., and Khorana, H. G. (1981) Refolding of an integral membrane protein. Denaturation, renaturation, and reconstitution of intact bacteriorhodopsin and two proteolytic fragments. *J. Biol. Chem. 256*, 3802−3809.
(14) Pervushin, K. V., Orekhov, V., Popov, A. I., Musina, L., and Arseniev, A. S. (1994) Three-dimensional structure of (1−71)-bacterioopsin solubilized in methanol/chloroform and SDS micelles determined by ^{15}N-^{1}H heteronuclear NMR spectroscopy. *Eur. J. Biochem. 219*, 571−583.
(15) Pan, Y., Brown, L., and Konermann, L. (2009) Mapping the structure of an integral membrane protein under semi-denaturing conditions by laser-induced oxidative labeling and mass spectrometry. *J. Mol. Biol. 394*, 968−981.
(16) Hawkins, C. A., de Alba, E., and Tjandra, N. (2005) Solution structure of human saposin C in a detergent environment. *J. Mol. Biol. 346*, 1381−1392.
(17) Yonath, A., Podjarny, A., Honig, B., Sielecki, A., and Traub, W. (1977) Crystallographic studies of protein denaturation and renaturation. 2. Sodium dodecyl sulfate induced structural changes in triclinic lysozyme. *Biochemistry 16*, 1418−1424.
(18) *The PyMOL Molecular Graphics System*, version 1.3r1 (2010) Schrodinger, LLC, New York.
(19) Tombolato, F., Ferrarini, A., and Freed, J. H. (2006) Dynamics of the nitroxide side chain in spin-labeled proteins. *J. Phys. Chem. B 110*, 26248−26259.
(20) Essen, L., Siegert, R., Lehmann, W. D., and Oesterhelt, D. (1998) Lipid patches in membrane protein oligomers: Crystal structure of the bacteriorhodopsin-lipid complex. *Proc. Natl. Acad. Sci. U.S.A. 95*, 11673−11678.
(21) Lanyi, J. K. (1992) Proton transfer and energy coupling in the bacteriorhodopsin photocycle. *J. Bioenerg. Biomembr. 24*, 169−179.
(22) Khorana, H. G., Gerber, G. E., Herlihy, W. C., Gray, C. P., Anderegg, R. J., Nihei, K., and Biemann, K. (1979) Amino acid sequence of bacteriorhodopsin. *Proc. Natl. Acad. Sci. U.S.A. 76*, 5046−5050.
(23) Khorana, H. G. (1988) Bacteriorhodopsin, a Membrane-Protein That Uses Light to Translocate Protons. *J. Biol. Chem. 263*, 7439−7442.
(24) Berendsen, H. J. C., Postma, J. P. M., van Gunsteren, W. F., and Hermans, J. (1981) Interaction models for water in relation to protein hydration. *Intermol. Forces,*, 331−342.
(25) Berendsen, H. J. C., Grigera, J. R., and Straatsma, T. P. (1987) The missing term in effective pair potentials. *J. Phys. Chem. 91*, 6269−6271.
(26) Darden, T., York, D., and Pedersen, L. (1993) Particle mesh Ewald: An N·log(N) method for Ewald sums in large systems. *J. Chem. Phys. 98*, 10089−10092.
(27) Essmann, U., Perera, L., Berkowitz, M., Darden, T., Lee, H., and Pedersen, L. (1995) A smooth particle mesh Ewald method. *J. Chem. Phys. 103*, 8577−8593.
(28) Berendsen, H. J. C., Postma, J. P. M., van Gunsteren, W. F., DiNola, A., and Haak, J. R. (1984) Molecular dynamics with coupling to an external bath. *J. Chem. Phys. 81*, 3684−3690.
(29) Hoover, W. G. (1985) Canonical dynamics: Equilibrium phase-space distributions. *Phys. Rev. A 31*, 1695−1697.
(30) Nosé, S. (2002) A molecular dynamics method for simulations in the canonical ensemble. *Mol. Phys. 100*, 191−198.
(31) Parrinello, M., and Rahman, A. (1981) Polymorphic transitions in single crystals: A new molecular dynamics method. *J. Appl. Phys. 52*, 7182−7190.
(32) Hess, B., Bekker, H., Berendsen, H. J. C., and Fraaije, J. G. E. M. (1997) LINCS: A linear constraint solver for molecular simulations. *J. Comput. Chem. 18*, 1463−1472.
(33) Hess, B. (2008) P-LINCS: A parallel linear constraint solver for molecular simulation. *J. Chem. Theory Comput. 4*, 116−122.
(34) Schuttelkopf, A. W., and van Aalten, D. M. F. (2004) PRODRG: A tool for high-throughput crystallography of protein-ligand complexes. *Acta Crystallogr. D60*, 1355−1363.
(35) van der Spoel, D., van Maaren, P. J., and Berendsen, H. J. C. (1998) A systematic study of water models for molecular simulation: Derivation of water models optimized for use with a reaction field. *J. Chem. Phys. 108*, 10220−10230.
(36) Sammalkorpi, M., Karttunen, M., and Haataja, M. (2007) Structural properties of ionic detergent aggregates: A large-scale molecular dynamics study of sodium dodecyl sulfate. *J. Phys. Chem. B 111*, 11722−11733.
(37) Schweighofer, K. J., Essmann, U., and Berkowitz, M. (1997) Simulation of sodium dodecyl sulfate at the water-vapor and water-carbon tetrachloride interfaces at low surface coverage. *J. Phys. Chem. B 101*, 3793−3799.
(38) van der Spoel, D., Lindahl, E., Hess, B., Kutzner, C., van Buuren, A. R., Apol, E., Meulenhoff, P. J., Tieleman, D. P., Sijbers, A. L. T. M., Feenstra, K. A., van Drunen, R., and Berendsen, H. J. C. (2006) *Gromacs User Manual*, version 4, University of Groningen, Groningen, The Netherlands.
(39) Humphrey, W., Dalke, A., and Schulten, K. (1996) VMD: Visual molecular dynamics. *J. Mol. Graphics 14*, 33−38.
(40) Griffiths, P. C., Paul, A., Heenan, R. K., Penfold, J., Ranganathan, R., and Bales, B. L. (2004) Role of counterion concentration in determining micelle aggregation: Evaluation of the combination of constraints from small-angle neutron scattering, electron paramagnetic resonance, and time-resolved fluorescence quenching. *J. Phys. Chem. B 108*, 3810−3816.
(41) Snider, C., Jayasinghe, S., Hristova, K., and White, S. H. (2009) MPEx: A tool for exploring membrane proteins. *Protein Sci. 18*, 2624−2628.
(42) Wimley, W. C., Creamer, T. P., and White, S. H. (1996) Solvation energies of amino acid side chains and backbone in a family of host-guest pentapeptides. *Biochemistry 35*, 5109−5124.
(43) Kabsch, W., and Sander, C. (1983) Dictionary of Protein Secondary Structure: Pattern-Recognition of Hydrogen-Bonded and Geometrical Features. *Biopolymers 22*, 2577−2637.
(44) Joh, N. H., Min, A., Faham, S., Whitelegge, J. P., Yang, D., Woods, V. L., and Bowie, J. U. (2008) Modest stabilization by most hydrogen-bonded side-chain interactions in membrane proteins. *Nature 453*, 1266−1273.
(45) Tulumello, D. V., and Deber, C. M. (2009) SDS Micelles as a Membrane-Mimetic Environment for Transmembrane Segments. *Biochemistry 48*, 12096−12103.
(46) Krishnakumar, S. S., and London, E. (2007) The control of transmembrane helix transverse position in membranes by hydrophilic residues. *J. Mol. Biol. 374*, 1251−1269.
(47) Luneberg, J., Widmann, M., Dathe, M., and Marti, T. (1998) Secondary structure of bacteriorhodopsin fragments: External sequence constraints specify the conformation of transmembrane helices. *J. Biol. Chem. 273*, 28822−28830.
(48) Mcleish, M. J., Nielsen, K. J., Najbar, L. V., Wade, J. D., Lin, F., Doughty, M. B., and Craik, D. J. (1994) Conformation of a Peptide Corresponding to T4 Lysozyme Residues 59−81 by NMR and CD Spectroscopy. *Biochemistry 33*, 11174−11183.
(49) Najbar, L. V., Craik, D. J., Wade, J. D., Lin, F., and Mcleish, M. J. (1995) CD and NMR Determination of the Solution Structure of a Peptide Corresponding to T4 Lysozyme Residues 38−51. *Biochim. Biophys. Acta 1250*, 163−170.

(50) Mammi, S., and Peggion, E. (1990) Conformational Studies of Human [15-2-Aminohexanoic acid]Little Gastrin in Sodium Dodecyl Sulfate Micelles by ^{1}H NMR. *Biochemistry 29*, 5265−5269.
(51) Rizo, J., Blanco, F. J., Kobe, B., Bruch, M. D., and Gierasch, L. M. (1993) Conformational Behavior of *Escherichia coli* Ompa Signal Peptides in Membrane Mimetic Environments. *Biochemistry 32*, 4881−4894.
(52) Son, H. S., and Sansom, M. S. (2000) Simulation studies on bacteriorhodopsin α-helices. *Eur. Biophys. J. 28*, 674−682.
(53) Woolf, T. B. (1997) Molecular dynamics of individual α-helices of bacteriorhodopsin in dimyristoyl phosphatidylcholine. 1. Structure and dynamics. *Biophys. J. 73*, 2376−2392.